Vacuum as a three-dimensional lattice of RLC cells. Derivation of the Wien and Hubble constants and relation to the cosmic microwave background (CMB) and the cosmic infrared background (CIB)

Gonzalo A. Moreno Jiménez[a)]
Faculty of Sciences, 14900. Cervantes, 24, Córdoba, Spain

(Received 5 November 2025; accepted 29 January 2026; published online 1 March 2026)

Abstract: The cosmological displacement of spectral lines observed in cosmic sources is conventionally attributed to their relative velocities. Nevertheless, this model evaluates the Hubble constant by considering that the propagation of time-varying electric and magnetic fields through the mathematical structure of the vacuum can itself produce a spectral redshift. To this end, the model describes the vacuum as a three-dimensional lattice of coupled RLC nodes in resonance. Each node functions as a discrete harmonic oscillator with quantized energy levels. This network of discrete components supports electromagnetic propagation in a manner characterized by its frequency. Within this framework, Wien's displacement constant arises naturally, providing it with a robust physical foundation, while the analysis also enables an examination of the vacuum's structure. By applying the model to a sample of galaxies and quasars, it reveals a possible connection between the cosmic microwave background and the cosmic infrared background, as well as discrepancies in the conventional distance estimates to certain quasars. Furthermore, the model suggests possible quantized values of H_0 spaced by 4.17 km s^{-1} Mpc^{-1}. The vacuum as a resonant network of discrete RLC nodes not only provides a physical derivation of the Wien and Hubble constants but also implies that such a deformable lattice could accommodate local space–time curvature and expansion. This perspective positions the structured vacuum as a promising framework for bridging cosmology with particle physics. © *2026 Physics Essays Publication*.
[http://dx.doi.org/10.4006/0836-1398-39.1.099]

Résumé: Le déplacement cosmologique des raies spectrales observé dans les sources cosmiques est conventionnellement attribué à leurs vitesses relatives. Néanmoins, ce modèle évalue la constante de Hubble en considérant que la propagation de champs électriques et magnétiques variables dans le temps à travers la structure mathématique du vide peut, en soi, produire un décalage spectral vers le rouge. À cette fin, le modèle décrit le vide comme un réseau tridimensionnel de nœuds RLC couplés en résonance. Chaque noeud fonctionne comme un oscillateur harmonique discret aux niveaux d'énergie quantifiés. Ce réseau de composants discrets permet la propagation électromagnétique d'une manière déterminée par sa fréquence. Dans ce cadre, la constante de la loi du déplacement de Wien émerge naturellement, lui fournissant une base physique robuste, tandis que l'analyse permet également un examen de la structure du vide. En appliquant le modèle à un échantillon de galaxies et de quasars, il révèle une connexion possible entre le fond diffus cosmologique (CMB) et le fond diffus infrarouge (CIB), ainsi que des divergences dans les estimations conventionnelles de distance pour certains quasars. De plus, le modèle suggère de possibles valeurs quantifiées de H_0 espacées de 4.17 km s^{-1} Mpc^{-1}. Le vide, conçu comme un réseau résonant de noeuds RLC discrètes, fournit non seulement une dérivation physique des constantes de Wien et de Hubble, mais implique également qu'un tel réseau déformable pourrait s'accommoder de la courbure locale et de l'expansion de l'espace-temps. Cette perspective positionne le vide structuré comme un cadre prometteur pour relier la cosmologie à la physique des particules.

Key words: RLC Lattice; Vacuum Electrodynamics; Hubble Constant; Cosmic Microwave Background (CMB); Cosmic Infrared Background (CIB); Cosmological Redshift; Vacuum Impedance; Vacuum Inductance; Fine–Structure Constant; Wien Wavelength Displacement Law Constant.

I. INTRODUCTION

I.1 When electromagnetic radiation propagates through space and its spectral lines exhibit a shift, this signifies an associated change in energy. The redshift z and the energy variation ΔE can both be expressed in terms of the observed wavelength λ and the emitted wavelength λ_e, as follows:

$$z = \frac{\lambda - \lambda_e}{\lambda_e}, \Delta E = -h\Delta\nu = ch\left(\frac{1}{\lambda_e} - \frac{1}{\lambda}\right) = \frac{ch}{\lambda}z. \quad (1)$$

a)email@gonzaloamoreno.com

I.2 Consider the *time-varying electric and magnetic components of an electromagnetic wave* with associated frequency ν. A time-varying electric field introduces a term in the Ampère–Maxwell law, representing a displacement current of magnitude,

$$\varepsilon \frac{d}{dt}\oint_S \mathbf{E}\cdot d\mathbf{S}. \tag{2}$$

From Gauss's law and Eq. (2), by differentiating the electric charge within a Gaussian surface S with respect to time, we obtain

$$\oint_S \mathbf{E}\cdot d\mathbf{S} = \frac{q}{\varepsilon}; \frac{dq}{dt} = I = \varepsilon \frac{d}{dt}\oint_S \mathbf{E}\cdot d\mathbf{S}. \tag{3}$$

Thus, in vacuum (i.e., in regions with charge density $\rho = 0$ and conduction current $\boldsymbol{J} = 0$), the Ampère–Maxwell law reduces to

$$\oint_L \mathbf{B}\cdot d\mathbf{L} = \mu_0\varepsilon_0 \frac{d}{dt}\oint_S \mathbf{E}\cdot d\mathbf{S}. \tag{4}$$

Within this framework, a photon can be regarded as a perturbation propagating through the vacuum. As it propagates, the mutually orthogonal, time-varying electric and magnetic fields of the electromagnetic wave carry the information.

Consequently, the vacuum can be modeled as a three-dimensional mesh of suitably configured, coupled RLC nodes. Each one functions as a discrete harmonic oscillator with quantized energy levels $E = (n + 1/2)h\nu$, so that the lattice conveys the $\boldsymbol{E}$ and $\boldsymbol{B}$ fields in a manner analogous to an electromagnetic wave characterized by its frequency ν. In this picture, the effective resistance R, inductance L, and capacitance C arise from the *intrinsic opposition to field variations* and from the vacuum's physico–mathematical constants, $\mu_0.l$, $\varepsilon_0.l$, together with the well-known characteristic impedance of free space $\Omega_0 = \sqrt{\mu_0/\varepsilon_0}$. The following sections develop this relationship in detail.

I.3 The energy change ΔE can be associated with the work performed on the wave between the time of emission t_e and the time of reception t_r,

$$\Delta E = W = \int_{te}^{t_r} I^2 Z dt. \tag{5}$$

Here, the impedance Z is defined in terms of the resistance R, the inductive reactance X_L, and the capacitive reactance X_C as $Z^2 = R^2 + (X_L - X_C)^2$. In a three-dimensional sequence of RLC nodes, the transmitted current I remains constant, and the vacuum quantity associated with that current that opposes changes in the magnetic field is the inductive reactance X_L. Thus, $Z_0 = X_L = L_0 2\pi\nu$. Combining this with the previous expressions, Eqs. (1), (3), (4), and (5), we deduce $\Delta E = \int_0^t (2\pi/\lambda) I_0^2 L_0 c dt = (ch/\lambda)z$, $z = f(D)$ ($D = ct$ is the distance traveled by the electromagnetic wave in vacuum).

$$z = \left(2\pi L_0 I_0^2/ch\right)D. \tag{6}$$

II. DERIVATION OF THE WIEN AND HUBBLE CONSTANTS

According to Hubble's law, the redshift z of a spectral line can be expressed as $z = H_0 D/c$. By comparing this with Eq. (6) derived in Section I.3, we obtain a relation for the Hubble constant,

$$L_0 I_0^2 = \hbar H_0. \tag{7}$$

This formula exhibits a formal similarity to the quantum energy of light $E = h\nu$, specifically to the term $2\pi L_0 I_0^2 = E_L$. Therefore, to derive the Hubble constant, we first analyze the energy term in Eq. (7), adopting the following fundamental premises:

1. The magnitude $I_0 = \varepsilon_0 \frac{d}{dt}\oint_S \mathbf{E}\cdot d\mathbf{S}$ must be intrinsically linked to the properties of the vacuum.
2. The vacuum inductance L_0 governs the time-varying magnetic component of the wave, and thus its propagation in free space, whose characteristic impedance is $\Omega_0 = \sqrt{\mu_0/\varepsilon_0}$.
3. As established above, we apply the energy relation for a harmonic oscillator, consistent with a discrete RLC node capable of producing and transmitting an electromagnetic wave in a vacuum. $E_H = (n + 1/2)h\nu$ for $n = 0, 1, 2, \ldots, n$.

These three premises are developed as follows.

II.1. Fundamentally, we define the relevant RLC attributes from the vacuum permittivity and permeability together with the minimal length and time scales, the Planck length $l_p = l_p^{(h)} = \sqrt{Gh/c^3}$ and the Planck time $t_p = l_p/c$.

$$\varphi L_0 = \mu_0 l_p; \quad \varphi C_0 = \varepsilon_0 l_p; \quad \varphi R_0 = \Omega_0 = \sqrt{\mu_0/\varepsilon_0}\ [ohm]. \tag{8}$$

For a single series RLC node operating at resonance, which emulates the behavior of the electromagnetic fields, the impedance is $Z = R + j(X_L - X_C)$, so the power factor, defined by $cos(\varphi)$, equals 1. This constrains the phase angle to $\varphi = n2\pi$, n = 0, 1, 2, … in Eq. (8), although the specific value of n must still be determined for the vacuum modeled as a three-dimensional lattice of RLC nodes. To that end, we evaluate φ by substituting the corresponding values for the resistance, inductive reactance, and capacitive reactance.

$$X_L = 2\pi\nu L\,;\ \nu = t_p^{-1} \Rightarrow X_{L0} = \mu_0 l_p/nt_p\,;\ X_{L0} = \Omega_0/n, \tag{9}$$

$$X_C = 1/2\pi\nu C\,;\ \nu = t_p^{-1} \Rightarrow X_{C0} = n\Omega_0, \tag{10}$$

$$R_0 = \Omega_0/n2\pi. \tag{11}$$

$\varphi = \arctan\left(\frac{X_L - X_C}{R}\right)$; $\varphi_0 = \arctan(2\pi(1 - n^2))$. Consequently, the unique value satisfying the discrete lattice constraints for Eqs. (9)–(11) is $n = 1$. It follows that the resulting vacuum parameter, the *vacuum inductance*, takes the form stated in the following equation:

$$L_0 = \Omega_0 t_p / 2\pi. \tag{12}$$

II.2. On the contrary, from the physical-mathematical generalization $1/(4\pi\varepsilon_0)q^2/r^2 = mc^2/r$ (note that the classical radius of the electron is given by $q = e$ and $m = m_e$), it is possible to define the spatial magnitude $r = q^2/(4\pi\varepsilon_0 mc^2)$. Coupling this scale with the Compton wavelength, $r = \lambda$, immediately leads us to the definition of an electric charge directly associated with free space. We refer to this vacuum property as the *unified charge* due to the consideration of this coupling, denoted as $q = q_p^{(h)} = q_U = \sqrt{4\pi h\sqrt{\varepsilon_0/\mu_0}} = \sqrt{4\pi h/\Omega_0}$. At this point, it is useful to note that the ratio between e and q_U is $e/q_U = \sqrt{\alpha/2\pi}$, which is fixed by the fine-structure constant α. It provides a convenient parametrization of the relation between the two charges: $\alpha = 2\pi(e/q_U)^2$. We now apply this significant value to the following equation:

$$\varepsilon_0 \frac{d}{dt}\oint_S \mathbf{E}\cdot d\mathbf{S} = I_0. \tag{13}$$

The angle between vectors $\boldsymbol{E}$ and $d\boldsymbol{S}$ is zero on the spherical surface that encloses the mathematical feature of the vacuum "unified electrical charge" in the transmission of electromagnetic waves,

$$I_0 = \varepsilon_0 \frac{d}{dt}\int_S \frac{q_U}{4\pi\varepsilon_0 r_0^2} dS\cos 0 = \frac{q_U}{4\pi}\frac{d}{dt}\left(\frac{r_0}{r_0^3}\right)4\pi r_0^2$$
$$= q_U \frac{dr_0}{dt}\frac{1}{r_0} = \frac{q_U c}{r_0}. \tag{14}$$

II.3. Regarding the value r_0 that satisfies the relation $I_0 r_0 = q_U c$ [as seen in Eq. (14)] in the 3-dimensional resonant RLC network, let us examine the expression for its dissipated power, $P_d = f(\varepsilon_{rms}, I_{rms}, \varphi)$; rms: root mean square in AC. To deduce the properties of this length scale quantity, we use Eq. (14) together with the previously obtained vacuum parameters, Eqs. (9)–(11) for n = 1: $X_{0L} = \Omega_0$, $X_{0C} = \Omega_0$, $R_0 = \Omega_0/2\pi$, $C_0 = t_p/(2\pi\Omega_0)$, and $L_0 = \Omega_0 t_p/2\pi$.

$$P_d = \varepsilon_{rms} I_{rms}\cos\varphi = I_{rms}^2 R, \quad P_d = (I_0/\sqrt{2})^2(\Omega_0/2\pi)$$
$$\rightharpoonup \quad P_d = c^2 h/r_0^2. \tag{15}$$

In this case, equating the dissipated power obtained under the stated premises, Eq. (15), to the total radiative power of a black body given by the Stefan–Boltzmann law, $P = \sigma A T^4$, naturally yields the relation between the wavelength of maximum emission and the temperature—namely, Wien's displacement law—now arising from a physical rather than purely mathematical deduction. More specifically, in general terms, the total power radiated by a black body may include an opacity or attenuation factor e^{-N}. Accordingly, the equality $\sigma 4\pi r_0^2 T^4 = e^{-N}c^2 h/r_0^2$ leads directly to **Wien's displacement law in physical terms**,

$$b = r_0 T = \sqrt[4]{\frac{c^2\hbar}{2\sigma}e^{-\Sigma}}. \tag{16}$$

Hence, r_0 coincides with Wien peak-emission wavelengths given by Wien's law, opening the possibility that the vacuum itself behaves as an effective black body. This allows the symbol r_0 to be replaced by λ_0 with no loss of meaning, merely a change in nomenclature. Anyway, to gauge the accuracy of Eq. (16), we compare its prediction with the CODATA Wien displacement constant,[1] as well as the relative error computed using the latest recommended values of c, h, and σ reported in the fundamental-constants database.

To evaluate this, we consider two baseline scenarios: (1) The zero-attenuation limit, N = 0. (2) A black-body framework with a specific value of $\sum$ obtained by treating the vacuum as a black body [see the derivation and physical interpretation of Eq. (16)], in which electromagnetic propagation occurs through a three-dimensional mesh of coupled RLC nodes forming a quantized lattice.

1. First path, $\Sigma = 0$ possibility. From Eq. (16), $b = 3.023\,56 \times 10^{-3}\,\mathrm{m\,K}$. The relative error is $E_r = 4.341\%$.
2. Second path. Comparing the theoretical Wien constant from Eq. (16) with the value derived mathematically from Planck's law, $b = ch/(xk_B)$, where $x = 4.965\,114\,231\,74$ is the solution to $x/(1 - e^{-x}) - 5 = 0$, indicates that $\Sigma \neq 0$. Moreover, because Boltzmann's constant and the Stefan–Boltzmann constant are related by $\sigma = (2\pi^5 k_B^4)/(15h^3c^2)$, there is a direct connection between Eq. (16) and $b = ch/(xk_B) = \sqrt[4]{(c^2h/\sigma)(2\pi^5/15x^4)}$. This equivalence not only supports the assumptions used in the derivation but also provides an opportunity to assign a physical meaning to x and to gain insight into the vacuum's internal structure.

- Evaluation of $\sum$ and its components.

Because the attenuation appears in exponential form, it can be expressed as a sum of contributions; that is, $\Sigma = F_1 + F_2 + \cdots + F_n$.

We now identify the individual contributions to $\sum$.

1. Let us denote N as the first attenuation factor, F_1, and examine its expression and value based on the premises adopted in this work and their consequences.

As previously discussed, a suitably arranged three-dimensional discrete RLC lattice conveys mutually orthogonal electric and magnetic fields throughout structured free space, each orthogonal to the longitudinal propagation axis $\boldsymbol{k}$ of the electromagnetic wave. However, the vacuum would transmit not only the two transverse fields but also a displacement–current density associated with the nodal charge $J_k = \epsilon_0 \cdot \partial\mathbf{E}/\partial t = 1/\mu_0 c \cdot \partial\mathbf{B}/\partial t$; $\partial\mathbf{E}/\partial t = c \cdot \partial\mathbf{B}/\partial t$ [J_k propagating along the longitudinal axis, as implied by Eqs. (13) and (14) together with the Ampère–Maxwell law]. This extra degree of freedom constitutes a longitudinal vacuum mode that alters the total emissive power without

changing the location of the spectral maximum determined by the transcendental x-equation in the dilute-coupling limit. Consequently, information transfer involves three possible polarizations in a vacuum: two mutually orthogonal transverse modes, both perpendicular to the propagation axis, and one longitudinal mode parallel to that axis.

Building on the connection established by Eq. (16) between the three-dimensional mesh of coupled RLC nodes and a black body, we can now evaluate the mode count in *k-space* for such a system. Specifically, the number of available states equals the number of polarizations multiplied by the ratio of the *k-space* volume element to the mode density $4\pi k^2 dk$,

$dN'(k) = 3 \cdot ((4\pi k^2 dk)/(2\pi)^3/V)$. Being the angular wave number in $\boldsymbol{k}$, $k = 2\pi\nu/c$ and $dk = (2\pi/c)d\nu$, $dN' = (V12\pi\nu^2/c^3)d\nu$.

Accordingly, the spectral density of states—that is, the number of electromagnetic modes per unit volume and per unit frequency—is defined as $g(\nu) = (1/V)(dN'/d\nu)$, so that for three polarizations it becomes

$$g(\nu) = \frac{12\pi\nu^2}{c^3}. \tag{17}$$

Multiplying the spectral density of states $g(\nu)$ defined by Eq. (17) by the average energy per mode of a quantum harmonic oscillator $\langle E\rangle = h\nu$, and by the Bose–Einstein occupation factor $\langle n\rangle$ yields the spectral energy density $u(\nu)$,

$$u(\nu) = g(\nu)h\nu\langle n\rangle = \frac{12\pi h}{c^3}\frac{\nu^3}{e^{h\nu/k_BT} - 1}. \tag{18}$$

Integrating the spectral energy density $u(\nu)$, Eq. (18) over all frequencies on $[0, \infty]$ and performing the change of variable $x = h\nu/(k_BT)$, one finds—after using the Riemann-zeta result $\zeta(4) = \pi^4/90$—that $u = (12\pi^5 k_B^4 T^4)/(15c^3h^3)$. Now, using the standard definition of the e Stefan–Boltzmann constant $\sigma = (2\pi^5 k_B^4)/(15c^2h^3)$, the total energy density can be written in compact form $u = 6\sigma T^4/c$.

We now connect this result with the standard black-body relations: The energy density takes the Stefan–Boltzmann form $u = aT^4$, with the radiation constant $a = 6\sigma/c$ corresponding to *three polarization modes*. The radiant exitance (power per unit area) equals $P_{d,S} = \sigma T^4$. Now, the power dissipated per unit volume can be written as $P_{d,V} = \alpha' cu$, where α' is the loss (absorption) coefficient linking energy density to radiative flux. Hence, $\alpha' = P_{d,V}/6\sigma T^4 = P_{d,S}/6l\sigma T^4$ for any length l, and the loss coefficient reduces to $\alpha' = 1/6l$.

We now relate α' to N in view of the physical meaning of the latter.

A wave undergoes an attenuation of N nepers when its magnitude decreases by a factor e^{-N} between two points along its path. $e^{-N} = \text{out}/\text{in} = x, N = -\ln(x)$. Equivalently, $N = \alpha' l$, since α' represents the attenuation per unit length. Taken together, these relations show that $\alpha' = -\ln(x)/l$ directly determines the exponent appearing in Eq. (16). Thus, combining $\alpha' = 1/6l$ with $N = \alpha' l$ yields the desired value

$$N = \frac{1}{6}. \tag{19}$$

2. Let us denote κ as the second attenuation factor, F_2. It is well known in solid-state physics that the fine-structure constant $\alpha = e^2/(4\pi\varepsilon_0 c\hbar)$ relates the characteristic impedance of free space to the von Klitzing quantum resistance R_k via the relation $Z/R_k = 2\alpha$. In the present setting, the analogy of the vacuum as a three-dimensional network of resonant RLC nodes—each surrounded by six nearest neighbors at the Planck scale, forming a fundamental unit for information transmission—leads to an attenuation factor in which the constant 2α is distributed across six directions. Therefore, based on this analogy adapted to the vacuum's three-dimensional network, κ takes the following value:

$$\kappa = \frac{2\alpha}{6}. \tag{20}$$

3. Let us denote δ as the third attenuation factor, F_3. Its evaluation requires further development of the framework, and its justification follows from the limiting energy-loss value implied by the three-dimensional network structure.

At this stage, we can fully develop Eq. (6). Taking into account the harmonic-oscillator energy introduced in Section II 3, $E_H = (n + 1/2)E_L$ and inserting the parameters evaluated in Eqs. (6), (7), (12), and (14), we obtain the following form for the redshift:

$$z = \left(n + \frac{1}{2}\right)\left(\Omega_0 l_p q_U^2/h\lambda_0^2\right)D = \left(n + \frac{1}{2}\right)\left(\frac{4\pi l_p}{\lambda_0^2}\right)D. \tag{21}$$

From this point onward, we examine the limiting value of this parameter within the three-dimensional network of nodes.

According to Eq. (21), the separation between adjacent levels follows the stated relation $\Delta z = (4\pi l_p D)/\lambda_0^2$. In the limiting case, we set $D = l_p$ and $\lambda_0 = \beta\eta l_p$, with $\beta = 1, 2, \ldots\eta$ and η denoting the number of nodes spanning β Planck lengths,

$$\Delta z_{(L)} = \frac{4\pi}{\beta^2\eta^2}. \tag{22}$$

Thus, for the minimal cell with $\eta = 7$ nodes satisfying $\beta = \eta$, distributing the effect once more across six directions yields δ from the limiting loss Δz shown in Eq. (22),

$$\delta = \frac{1}{6}\Delta z_{(L)} = \frac{1}{6}\frac{4\pi}{7^4}. \tag{23}$$

4. Let us denote γ as the fourth attenuation factor, F_4. Its construction is based on the following considerations: Known particles emerge as oscillatory solutions of the quantum vacuum lattice; therefore, the statistical and resonant properties of the network must reflect the corresponding mass and

charge ratios. Because both properties arise from the vacuum structure, the way it transmits or attenuates electromagnetic energy must implicitly encode these proportions. Once again, the information is divided among the six directions of the three-dimensional network. This leads to a product of ratios that serves as a probabilistic estimate consistent with these conditions,

$$\gamma = \frac{1}{6}\cdot\frac{e}{q_U}\left(\frac{m_n}{m_p}\right)^{12}\frac{m_e}{m_p}. \tag{24}$$

For clarity, let $M_{n,p}$ denote the known neutron-to-proton mass ratio, and $M_{e,p}$ the electron-to-proton mass ratio. Likewise, as shown in Section II 2, the ratio of the electric charges e and q_U can be expressed in terms of the fine-structure constant: $e/q_U = \sqrt{\alpha/2\pi}$. Thus, in this notation, Eq. (24) remains,

$$\gamma = \frac{1}{6}\sqrt{\frac{\alpha}{2\pi}}M_{n,p}^{12}M_{e,p}. \tag{25}$$

Finally, with these four parameters we can calculate $\sum$. Recall that $\Sigma = F_1 + F_2 + \cdots + F_n$ and, with the present notation, $\Sigma = N + \kappa + \delta + \gamma$. Substituting the expressions obtained above [Eqs. (19), (20), (22), (23), and (25)] yields the final result,

$$\Sigma = \frac{1}{6}\left(1 + 2\alpha + \frac{4\pi}{7^4} + \sqrt{\frac{\alpha}{2\pi}}M_{n,p}^{12}M_{e,p}\right). \tag{26}$$

Using these inputs, the final value of the constant $b = r_0T$ and its relative error, computed with respect to the fundamental constants listed in the CODATA database, are as follows:

- Codata 1: Electron–proton mass ratio (concise form), $m_e/m_p = 5.446\,170\,214\,889(94) \times 10^{-4}$; neutron–proton mass ratio, $m_n/m_p = 1.001\,378\,419\,46(40)$; and fine-structure constant, $\alpha = 7.297\,352\,564\,3(11) \times 10^{-3}$. $\sum$ depends on dimensionless constants $\{\alpha, m_e/m_p, m_n/m_p\}$ whose relative uncertainties are $\lesssim 10^{-10}$. Consequently, $\delta b/b \lesssim 10^{-10}$.
  Wien displacement law constant, $b = 2.897\,771\,955\ldots \times 10^{-3}$[mK].
- Equations (16) and (26): $b = 2.897\,771\,955 \times 10^{-3}$[mK]. Relative error to 12 decimal places: $E_r = 0$—exact agreement.

In other words, *the discrete-vacuum framework provides a physical derivation of the Wien displacement constant* [Eqs. (16) and (26)]. *The resulting value of "b" is in exact agreement with the reference value.*[1]

II.4 Hubble Constant. Mathematical form: We now return to the goal of this section: Deriving a mathematical expression for the Hubble constant from the quantized-vacuum framework. In fact, it follows from the z term in Eq. (21), and after a series of straightforward steps with $l_p = l_p^{(h)} = \sqrt{Gh/c^3}$, we obtain the following result:

$$H_0 = \left(n + \frac{1}{2}\right)\left(\Omega_0 l_p c q_U^2/h\lambda_0^2\right) = \left(n + \frac{1}{2}\right)\left(\frac{4\pi l_p c}{\lambda_0^2}\right). \tag{27}$$

We must now specify λ_0. As shown above, r_0 satisfies Wien's displacement law. Therefore, the most suitable choice is the peak wavelength of the cosmic microwave background (CMB), which permeates the observable universe with high uniformity. In this case, Wien's law gives $\lambda_{\max}$ through $\lambda_{\max}T = b$ with $T = 2.725\,48 \pm 0.000\,57$K,[1–3] yielding $\lambda_{\max} = \lambda_0 = 1.0632 \times 10^{-3}$m. We then use this value and consider the allowed values of the quantum number n. Equation (27), therefore, yields a discrete set of H_0 values. The values listed in Table I are expressed in km s^{-1} Mpc^{-1}. Physical constants are taken from CODATA 2022.[1] Note that these H_0 values could change materially with updated CMB temperature measurements and slightly with revisions of the fundamental constants. In any event, successive levels differ by a constant difference of $4.1662(2) \sim 4.17$ km s^{-1} Mpc^{-1}.

The values computed for $n = 13$–19 in Table I are highlighted to emphasize those theoretical H_0 estimates that align with the bulk of current experimental determinations. For reference, Fig. 1 compares the range of H_0 values from Eq. (27) (Table I) with recent high-quality measurements.

III. APPLICATIONS AND CONNECTIONS

The self-inductive model developed here applies to any source that emits electromagnetic radiation into vacuum. We now apply it to cosmic-size sources—galaxies and quasars—to search for possible differences in the Hubble constant and, if present, to identify an underlying distinguishing parameter. Some authors have argued for physical associations between certain quasars and nearby galaxies, in tension with the conventional distance assignments to some quasars, but this hypothesis provides a useful test bed for investigating a potential distinguishing parameter, which must subsequently be corroborated observationally.

TABLE I. H_0 theoretical values.

n	H_0 (km s^{-1} Mpc^{-1})	n	H_0 (km s^{-1} Mpc^{-1})
0	2.08	14	*60.42*
1	6.25	15	*64.58*
2	10.42	16	*68.75*
3	14.58	17	*72.92*
4	18.75	18	*77.08*
5	22.91	19	*81.25*
6	27.08	20	85.42
7	31.25	21	89.58
8	35.41	22	93.75
9	39.58	23	97.92
10	43.75	24	102.07
11	47.92	25	106.24
12	52.08	26	110.40
13	*56.25*	27	114.57

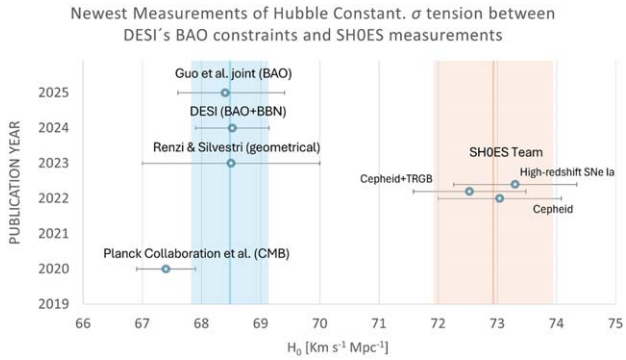

FIG. 1. (Color online) Recent estimates of the Hubble constant compiled from Guo *et al*.[4] The figure includes the value derived from the latest baryon acoustic-oscillation (BAO) data released by the Dark Energy Spectroscopic Instrument (DESI) survey. The figure also shows the most significant recent estimates obtained with the Hubble Space Telescope by the SH0ES collaboration.[5] It also includes the estimate reported by Renzi and Silvestri from a joint analysis of independent geometric datasets;[6] the Planck Collaboration 2020 result based on CMB observations,[7] and the latest DESI Collaboration determination obtained from combined BAO + BBN data.[8]

Considering the redshift data in Table II, we take into account the probability of association.[9] Applying the model with the association of the parameters D: distance covered by the electromagnetic wave, n: quantum number of the harmonic oscillator, and z: experimental redshift, to each source results in the following:

1. Source: Use D_1, n_1, z_1 with $\lambda_0 = \lambda_{01} = \lambda_{\max}(\mathrm{CMB})$.
2. Associated structure(s) in Table II: Use D_2, n_2, z_2 with $\lambda_0 = \lambda_{02}$ defined accordingly.

Setting $D_1 = D_2$ and $n_1 = n_2$ in Eq. (21) yields the relation stated in the following equation:

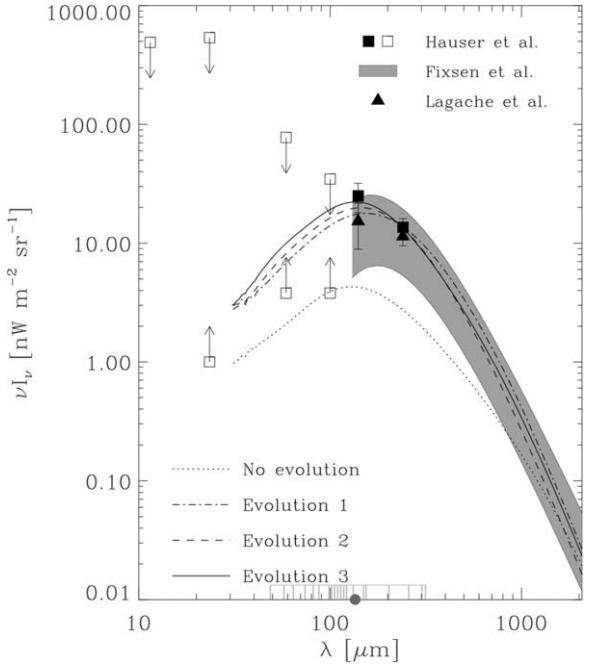

FIG. 2. Cosmic infrared background (CIB) spectrum. Vertical markers along the x axis indicate the values of λ_{02} obtained from Eq. (28) and Table II, while the filled dot represents their average, $\overline{\lambda_{02}} = \lambda_{\max}$. The distribution of λ_{02} predicted by the RLC model under the stated hypothesis agrees with the observational data within uncertainties.[10–13]

$$\lambda_{02} = \lambda_{01}\sqrt{\frac{z_1}{z_2}}. \tag{28}$$

Table II reports the galaxy and quasar redshifts together with the corresponding λ_{02} values. The first key point is that the λ_{02} values align well with the cosmic infrared background (CIB) spectrum. The distribution of λ_{02} closely

TABLE II. Experimental redshift distribution.

		Reference 9					Equation (28)
	GALAXY	z_1	QUASAR	z_2	z_1/z_2	Δz	λ_{02} (μm)
1	NGC 622	0.018	UB1	0.91	0.0198	0.89	149.5
2			BSO1	1.46	0.0123	1.44	118.1
3	NGC 470	0.009	68	1.88	0.0048	1.87	73.6
4			68 D	1.53	0.0059	1.52	81.5
5	NGC 1073	0.004	BSO1	1.94	0.0021	1.94	48.3
6			BSO2	0.60	0.0067	0.60	86.8
7			RSO	1.40	0.0029	1.40	56.8
8	NGC 3842	0.02	QSO1	0.34	0.0588	0.32	257.9
9			QSO2	0.95	0.0211	0.93	154.3
10			QSO3	2.20	0.0091	2.18	101.4
11	NGC 4319	0.0057	MARK 205	0.07	0.0814	0.06	303.4
12	MCG03-34–85	0.018	PKS-1327–206	1.17	0.0154	1.15	131.9
13	NGC 5296	0.0083	BSO#1	0.96	0.0086	0.95	98.9
14	3C 303	0.14	UVHC	1.57	0.0892	1.43	317.5
15	1C 2402	0.0667	0844 + 31	1.83	0.0364	1.76	203.0
16	0924 + 30	0.0267	COMPACT SOURCE	2.02	0.0132	1.99	122.2
17	NGC 520	0.00758	⋯	0.77	0.0098	0.76	105.5
18			⋯	0.67	0.0113	0.66	113.1
19			⋯	2.11	0.0036	2.10	63.7
20			⋯	0.72	0.0105	0.71	109.1
					(z_1/z_2)max		Average
					0.089		134.8 μm

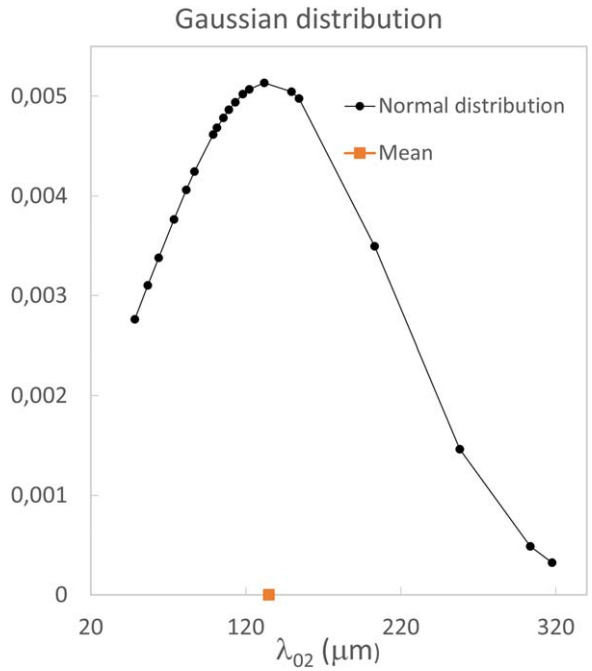

FIG. 3. (Color online) The normal distribution for λ_{02} data fits to a blackbody distribution in accordance with the CIB with an approximate temperature of 21.5 K.[14]

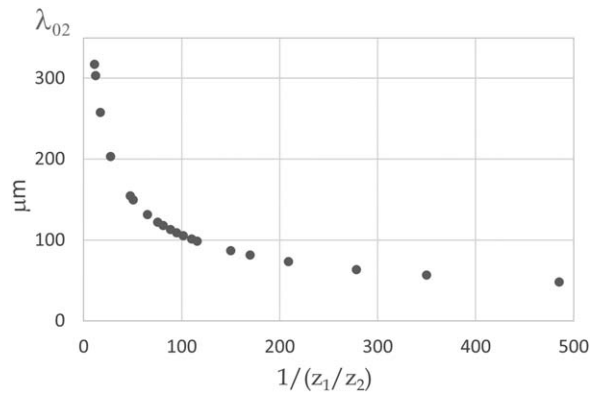

FIG. 4. Representation of the wavelength $\lambda_{02} = \lambda_{01}\sqrt{z_1/z_2}$. Note the orderly distribution and the enhanced concentration arising from the nonaccidental associations (Table II).[9]

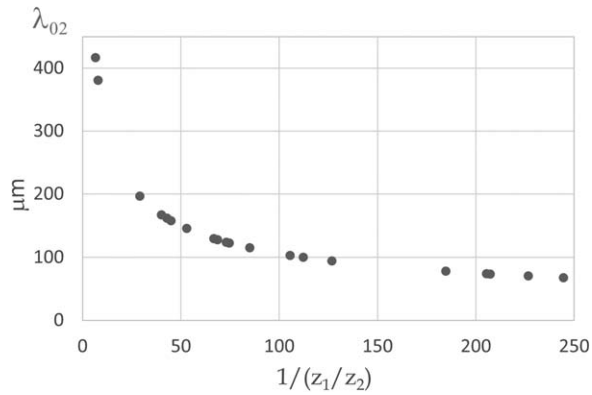

FIG. 5. Random association of the samples from Table III. The sampling illustrates the irregular distribution that results from random association, in contrast with the classification used for the nonrandom case (Fig. 4).

TABLE III. Random Z_1, Z_2 association.

	z_1	z_2
1	0.018	0.77
2		0.72
3		0.95
4		2.02
5	0.009	0.60
6		2.20
7		0.07
8		0.67
9	0.02	2.11
10		1.46
11	0.005 7	1.17
12	0.018	1.53
13	0.008 3	1.88
14	0.14	0.91
15	0.066 7	1.94
16	0.026 7	1.83
17	0.007 58	1.57
18		0.96
19		0.34
20		1.40

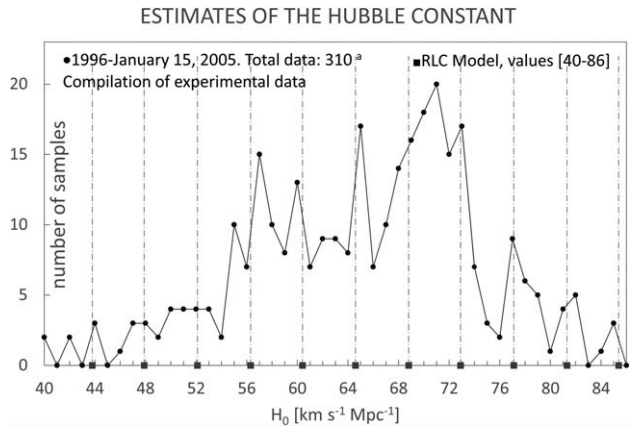

FIG. 6. The ordinate shows the number of H_0 measurements reported between 1996 and the latest update of the source[b)] included in Ref. 14. Despite measurement uncertainties, the experimental values cluster around those predicted by the model, forming peaks at or near the theoretical levels. This representation highlights possible global patterns in the behavior of H_0; its robustness improves as additional data accumulate, notwithstanding individual measurement inaccuracies. Indeed, the graph suggests *multiple possible quantized values* of H_0 separated by 4.1 km s^{-1} Mpc^{-1} (Table IV), which closely coincides with the model predicted value 4.17 km s^{-1} Mpc^{-1}.

matches the experimental CIB distribution. These comparisons are shown in Fig. 2. The data also show close agreement between the arithmetic mean of $\overline{\lambda}_{02}$ and the maximum of the experimental CIB spectrum (Fig. 3). The data contained in Table III has been randomly rearranged from the contents of Table II to illustrate consistencies in Figure 4 from Table II, and possible inconsistencies in Figure 5 from Table III. Table IV illustrates the pattern derived from the experimental data presented in Figure 6.

[b)]J. Huchra, "Estimates of the Hubble Constant." https://lweb.cfa.harvard.edu/~dfabricant/huchra/, https://lweb.cfa.harvard.edu/~dfabricant/huchra/hubble.plot.dat

TABLE IV. Statistics for H_0 [km s^{-1} Mpc^{-1}].

	Reference 1			
	Source: Harvard-Smithsonian Center for Astrophysics. John Huchra			RLC model
	Peak points formation (experimental H_0 values)	Average	Peak points difference $N, N-1$	H_0 values
1	43, 44, 45	44.0		43.75
2	45, 46, 47, 48, 49	47.0	3.0	47.91
3	49, 50, 51, 52, 53, 54	51.5	4.5	52.08
4	54, 55, 56, 57, 58, 59	56.5	5.0	56.24
5	59, 60, 61	60.0	3.5	60.41
6	61, 62, 63, 64, 65, 66	63.5	3.5	64.58
7	66, 67, 68, 69, 70, 71, 72	69.0	5.5	68.74
8	72, 73, 74, 75, 76	74.0	5.0	72.91
9	76, 77, 78, 79, 80	78.0	4.0	77.08
10	80, 81, 82, 83	81.5	3.5	81.25
11	83, 84, 85, 86	84.5	3.0	85.42
			$\overline{\Delta H}_0 = 4.1$	$\Delta H_0 = 4.17$

IV. CONCLUSIONS AND INTERPRETATIONS

This section summarizes the main insights drawn from the preceding developments and the experimental data.

The vacuum as a three-dimensional mesh of RLC nodes provides a coherent framework for explaining the behavior of electric and magnetic fields and, consequently, the transmission of electromagnetic waves. Within this perspective, the framework offers a physical setting that relates phenomena initially considered disconnected, such as the formation and transmission of these fields based on the physico-mathematical properties of the vacuum, as well as a possible connection between the vacuum and black-body behavior characterized by polarization count and quantization. Evidence for this close relationship is that the premise yields a physical interpretation of the Wien displacement constant. Although this constant is usually obtained as a mathematical consequence of Planck's law, in contrast, here it emerges naturally from the development of the equations under the stated conditions. Moreover, its derivation and calibration imply several novel elements: The need for a third polarization associated with the vacuum displacement current $\boldsymbol{J_k}$ arising from the discrete resonant RLC network; the presence of geometric and structural factors—such as $\delta = 1/6\Delta z_{(L)}$—capable of producing physical effects; and the incorporation, within the oscillator network, of ratios consistent with probabilistic estimates and the emergent properties of particles, among others.

Once time-varying electromagnetic fields propagate through the network of coupled RLC nodes—equivalent to quantum harmonic oscillators—the relations among the vacuum's physico-mathematical constants $(\epsilon_0, \mu_0, G, h, \ldots)$ systematically and subtly *oppose changes* in the field magnitudes within the three-dimensional structure. In this way, the relationship between cosmological redshift and these intrinsic properties arises. Indeed, this connection links a quantity as central to physics and cosmology as the Hubble constant to the discrete three-dimensional structure of the vacuum. The wavelength $r_0 = \lambda_0$ appears to connect the intrinsic cosmic redshift with the cosmic backgrounds. This value remains constant along the electromagnetic wave's trajectory but depends on the source, with $E_H = hH_0$ and $H_0 = f(n, \lambda_0)$.

The vacuum, modeled as a quantum network of resonantly coupled nodes, does not exclude the possibility of local space–time curvature or expansion. On the contrary, the inherent deformability of such a discrete lattice suggests that it could accommodate geometric deformations while preserving its fundamental structure. This feature positions the framework as a strong candidate for bridging cosmology and particle physics, offering a potential unifying perspective across the largest and smallest physical scales.

The foregoing can be summarized in a tentative conclusion: The term *crystallization* may merit consideration within cosmological terminology. Such a concept may offer a useful perspective on the vacuum's discrete, structured nature, suggesting an ordered framework underlying fundamental cosmic phenomena in a self-driven universe, without precluding further investigation or alternative interpretations.

[1]P. J. Mohr, D. B. Newell, B. N. Taylor, and E. Tiesinga, arXiv:2409.03787 (2024).
[2]D. J. Fixsen, Astrophys. J. **707**, 916 (2009).
[3]D. J. Fixsen, E. S. Cheng, J. M. Gales, J. C. Mather, R. A. Shafer, and E. L. Wright, Astrophys. J. **473**, 576 (1996).
[4]W. Guo, Q. Wang, S. Cao, M. Biesiada, T. Liu, Y. Lian, X. Jiang, C. Mu, and D. Cheng, Astrophys. J. Lett. **978**, L33 (2025).
[5]SH0ES Team, Astrophys. J. Lett. **934**, L7 (2022).
[6]F. Renzi and A. Silvestri, Phys. Rev. D **107**, 023520 (2023).
[7]Planck Collaboration Group, Astron. Astrophys. **641**, A6 (2020).
[8]DESI Collaboration, arXiv:2404.03002 [astro-ph] (2024).
[9]H. Arp, *Controversias Sobre Las Distancias Cósmicas y Los Cuásares (Controversies about Cosmic Distances and Quasars)*. Metatemas 27 (Tusquets Editores, Barcelona, 1992).
[10]M. G. Hauser, R. G. Arendt, T. Kelsall, E. Dwek, N. Odegard, J. L. Weiland, H. T. Freudenreich, W. T. Reach, R. F. Silverberg, S. H. Moseley, Y. C. Pei, P. Lubin, J. C. Mather, R. A. Shafer, G. F. Smoot, R. Weiss, D. T. Wilkinson, and E. L. Wright, Astrophys. J. **508**, 25 (1998).
[11] D. J. Fixsen, E. Dwek, J. C. Mather, C. L. Bennett, and R. A. Shafer, Astrophys. J. **508**, 123 (1998).
[12]G. Lagache, Ph.D. thesis (Université Paris XI, Orsay, 1998).
[13]T. T. Takeuchi, T. T. Ishii, H. Hirashita, K. Yoshikawa, H. Matsuhara, K. Kawara, and H. Okuda, arXiv:astro-ph/0009460 (2000).
[14]G. A. Moreno, Galilean Electrodyn. **19**, 5 (2008).